

# Synthetic Butterfly Scale Surfaces with Compliance-Tailored Anisotropic Drop Adhesion

Hangbo Zhao, Sei Jin Park, Brian R. Solomon, Sanha Kim, Dan Soto, Adam T. Paxson, Kripa K. Varanasi,\* and A. John Hart\*

Many natural surfaces such as butterfly wings, beetles' backs, and rice leaves exhibit anisotropic liquid adhesion; this is of fundamental interest and is important to applications including self-cleaning surfaces, microfluidics, and phase change energy conversion. Researchers have sought to mimic the anisotropic adhesion of butterfly wings using rigid surface textures, though natural butterfly scales are sufficiently compliant to be deflected by capillary forces exerted by drops. Here, inspired by the flexible scales of the *Morpho aega* butterfly wing, synthetic surfaces coated with flexible carbon nanotube (CNT) microscales with anisotropic drop adhesion properties are fabricated. The curved CNT scales are fabricated by a strain-engineered chemical vapor deposition technique, giving  $\approx 5000$  scales of  $\approx 10\ \mu\text{m}$  thickness in a  $1\ \text{cm}^2$  area. Using various designed CNT scale arrays, it is demonstrated that the anisotropy of drop roll-off angle is influenced by the geometry, compliance, and hydrophobicity of the scales; and a maximum roll-off anisotropy of  $6.2^\circ$  is achieved. These findings are supported by a model that relates the adhesion anisotropy to the scale geometry, compliance, and wettability. The electrical conductivity and mechanical robustness of the CNTs, and the ability to fabricate complex multidirectional patterns, suggest further opportunities to create engineered synthetic scale surfaces.

Engineering of synthetic surfaces with anisotropic wetting or adhesion allows liquids to be directed passively, enabling new concepts for self-cleaning surfaces,<sup>[1]</sup> contact-based adhesives,<sup>[2,3]</sup> and low-cost flow manipulation for diagnostics.<sup>[4]</sup> A great inspiration is found in nature, where many plants and animals exhibit anisotropic wetting or liquid transport on their skin/surface, arising from anisotropic textures such as those found on pitcher plant rims,<sup>[5]</sup> rice leaves,<sup>[6]</sup> water strider

legs,<sup>[7]</sup> and butterfly wings,<sup>[8,9]</sup> etc. In particular, certain species of butterflies such as *Morpho aega* (*M. aega*) have wings that are decorated with imbricate microscales. Their wings exhibit directional drop adhesion whereby a drop rolls off the wing surface much more easily in the direction away from the body than in the direction towards the body.<sup>[8]</sup> In addition, the surface of each *M. aega* scale is decorated with multilayer nanoscale ridges, which contributes to the superhydrophobicity of the surface and causes light diffraction and interference, giving rise to iridescent structural colors.<sup>[10]</sup>

Inspired by the anisotropic wetting and adhesion properties of butterfly wings and other natural surfaces like rice leaves, biomimetic engineering has applied fabrication methods including lithography, deposition, self-assembly, wrinkling, and replica molding to mimic natural surface structures and textures.<sup>[11–13]</sup> Previous efforts to fabricate anisotropic surfaces include 1D or 2D grooved surfaces,<sup>[4,14]</sup> 3D structured surfaces composed of slanted pillars/wires or hierarchical


textures,<sup>[6,15–19]</sup> and direct replication of natural surfaces using replica molding.<sup>[20,21]</sup> Nevertheless, almost all of these artificial surfaces exhibit anisotropic wetting or adhesion properties entirely from the geometric anisotropy of rigid surface textures.

However, it was recently found that the anisotropic adhesion of *M. aega* butterfly wings is due to the deflection of microscales enabled by their compliance,<sup>[22]</sup> and therefore the surface does not behave as a rigid ratchet. Moreover, compliant hairs on certain plants and animals have been shown to influence liquid behaviors. For instance, the flexible water strider's leg hairs allow for self-removal of condensed water by elastically expelling drops out of the hairs,<sup>[7]</sup> and generation of anisotropic adhesive forces to facilitate locomotion on water.<sup>[16]</sup> Here, we show that the compliance-derived anisotropy of butterfly wings can be mimicked using flexible synthetic microscales, which are fabricated by directional growth of carbon nanotube (CNT) microstructures, opening up new possibilities for bioinspired surface engineering.

The design of the CNT scale surfaces is based on the geometry of *M. aega* butterfly wings, as shown in **Figure 1**. *M. aega* butterfly wings are superhydrophobic (**Figure 1a**), and have directional drop adhesion due to the deflectable microscales,<sup>[8,22]</sup> (**Figure 1b**). The microscales are  $\approx 180\ \mu\text{m}$  long,  $70\ \mu\text{m}$  wide,

Dr. H. Zhao, Dr. S. J. Park, Dr. B. R. Solomon, Dr. S. Kim, Dr. D. Soto, Dr. A. T. Paxson, Prof. K. K. Varanasi, Prof. A. J. Hart  
Department of Mechanical Engineering and Laboratory  
for Manufacturing and Productivity  
Massachusetts Institute of Technology  
Cambridge, MA 02139, USA  
E-mail: kripa@mit.edu; ajhart@mit.edu

Dr. S. J. Park  
Physical and Life Sciences Directorate  
Lawrence Livermore National Laboratory  
7000 East Avenue, Livermore, CA 94550, USA

 The ORCID identification number(s) for the author(s) of this article can be found under <https://doi.org/10.1002/adma.201807686>.

DOI: 10.1002/adma.201807686

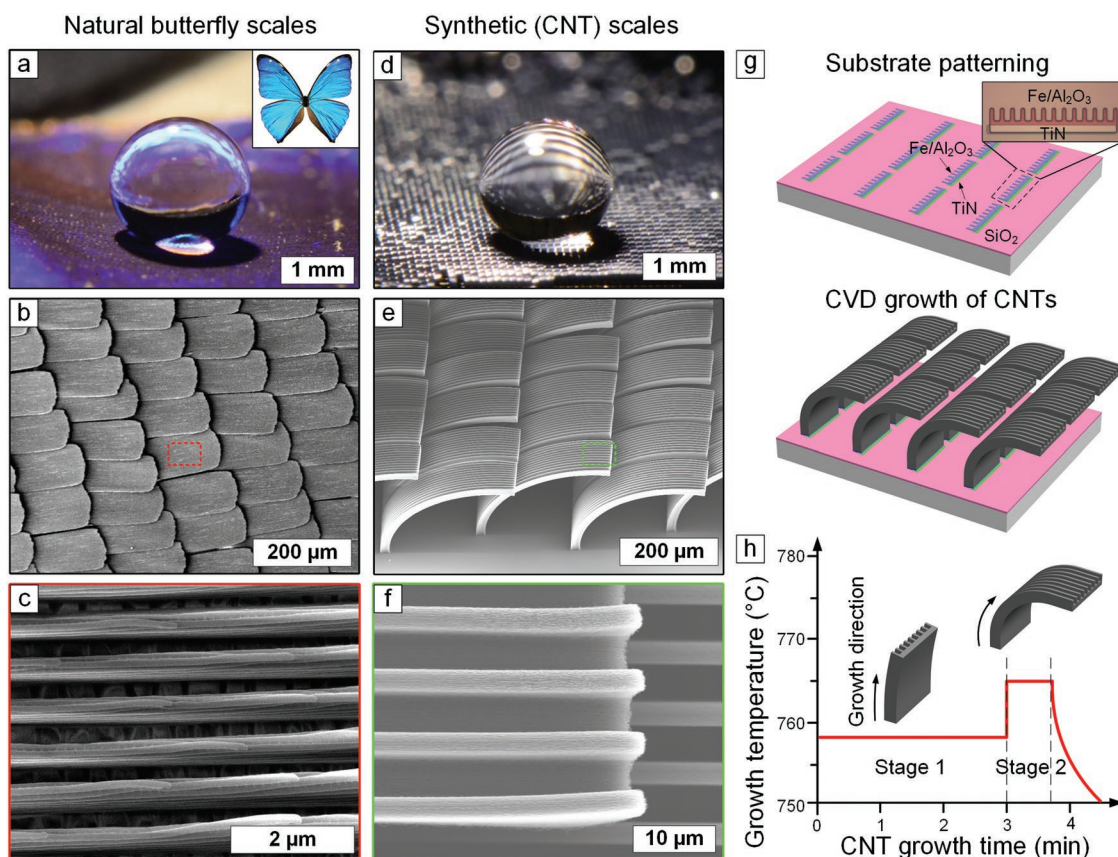


**Figure 1.** Butterfly-inspired scale surfaces with anisotropic drop adhesion. a–c) and d–f) Corresponding optical and SEM images of *M. aega* butterfly scales and synthetic CNT scales fabricated by strain-engineered chemical vapor deposition. g) Schematic of the fabrication process of synthetic scale surfaces: catalyst ( $\text{Fe}/\text{Al}_2\text{O}_3$ )/underlayer (TiN) offset pattern and growth of CNTs into curved microscale arrays. The scale surface becomes superhydrophobic upon a conformal coating of DVB on the CNTs. h) Temperature profile of segmented CNT growth resulting in slight curvature in stage 1 and sharp curvature in stage 2.

and 3  $\mu\text{m}$  thick. The surfaces of the microscales are decorated with nanoscale ridges (Figure 1c). Inspired by this unique *M. aega* wing geometry, we fabricate synthetic scale arrays comprising thin, curved CNT microstructures coated with a hydrophobic polymer. The synthetic surface is superhydrophobic (Figure 1d) due to the hydrophobic coating and its multiscale texture (Figure 1e,f). The synthetic scales appear dark due to the strong light absorption of CNTs omnidirectionally,<sup>[23,24]</sup> and structural color can be achieved on nanopatterned, high density CNT forests.<sup>[25]</sup>

CNT scales are produced by patterning a thin film catalyst for CNT growth, where the cross-section of each scale is simplified as a rectangle with ridges (Figure 1g). Using a strain-engineered chemical vapor deposition (CVD) technique,<sup>[26,27]</sup> CNT growth is programmed to spatially vary across the width of each scale, causing the scales to curve directionally. The fabrication process starts with patterning a growth retardant TiN layer, followed by patterning a CNT catalyst layer ( $\text{Fe}/\text{Al}_2\text{O}_3$ ) on top. To make the scale pattern, large arrays of  $\approx 10\ \mu\text{m}$  wide, comb-shaped patterns which partially overlap with the underlying TiN layer (Figure S1, Supporting Information) are fabricated. The dimensions of the catalyst pattern are designed to resemble the geometry of the *M. aega* butterfly microscales. Note that the patterned ridges are 3  $\mu\text{m}$  wide instead of

submicrometer as on the *M. aega* wings in order to maintain compatibility of the process with standard photolithography for catalyst patterning. After substrate patterning, the CNT “forest” grows within the catalyst area of each scale cross-section. Thus, uniform arrays of curved microscales are formed ( $\approx 10\ \mu\text{m}$  thick,  $\approx 5000\ \text{scales cm}^{-2}$ ), with micrometer ridges on their upward facing surface.

The height and curvature of the CNT scales are controlled by the parameters of the CVD process, including the growth time and temperature. The ratio of CNT forest growth rates from  $\text{Fe}/\text{Al}_2\text{O}_3$  catalyst on TiN and  $\text{SiO}_2$  (non-TiN area) is inversely proportional to temperature, and decreases from 0.95 to 0.63 as the growth temperature increases from 755 to 800  $^\circ\text{C}$  (Figure S2, Supporting Information).<sup>[27]</sup> Thus, a higher CNT growth temperature results in a higher curvature within this temperature range. To fabricate the scales, we change the temperature during growth such that the first (upper) portion of the scales is only slightly curved, while the lower portion is highly curved, resulting in overlapping but rather flat scale geometries which give a greater liquid–solid contact area than curved scales. The shapes of the CNT scales can be predicted by a step-wise finite element method (FEM) simulation (Figure S3, Supporting Information)<sup>[27]</sup> which considers the growth rates of the CNT forests and their mechanical properties.

The CNT scales must be modified to impart scale-like wetting properties, because water can wick into as-grown CNT structures and cause CNT densification due to elastocapillary effects.<sup>[28–31]</sup> A thin hydrophobic polymer divinylbenzene (DVB) is conformally coated onto the CNT scale surfaces via an initiated chemical vapor deposition (iCVD) process (Figure S4, Supporting Information).<sup>[31,32]</sup> Advancing and receding contact angles of  $\approx 91^\circ$  and  $73^\circ$  are measured from flat DVB films (Figure S5, Supporting Information). The DVB-coated scale surfaces exhibit superhydrophobicity due to the microscale ridge textures and the inherent nanoscale roughness in the CNTs (Movie S1, Supporting Information). The ridges enhance the hydrophobicity of the scales by reducing the fraction of solid surface area wetted by the liquid drop in the Cassie-Baxter state.<sup>[33]</sup>

The difference between the roll-off angle of a water drop in the direction toward the CNT scales (along the scale bending direction) and against the scales (opposite to the scale bending direction) is measured to evaluate the adhesion anisotropy. Video microscopy is used to observe the contact line between a water drop and the scales as it rolls over the scales, as shown in Figure 2a,b; Figures S6 and S7 and Movie S2 in the Supporting Information. As a drop rolls against the scales, the scales are pulled by the drop pinning force (Figure 2a). After the scales deflect to a certain degree, the restoring force of the scales exceeds the pinning force and brings the scales back to their original positions. This pinning–depinning process continues as the drop moves over the array of scales and makes contact with the subsequent scales in its moving direction. However, when the drop rolls toward the scales, no visible deflection is observed (Figure 2b).

Thus, DVB-coated CNT scales (Figure S7, Supporting Information) show small anisotropy, with roll-off angles of  $3.4^\circ$  toward the scales and  $6.7^\circ$  against the scales. To increase scale compliance and modulate the anisotropy, the CNT scales are mechanically compressed after CNT growth and DVB coating. This kinks the scales near their base (Figure 2c), emulating another important feature of *M. aega* scales which are attached to the wing by flexible posts.<sup>[22]</sup> On folded CNT scales, the roll-off angles are measured to be  $11.6^\circ$  toward scales and  $17.8^\circ$  against scales, giving  $6.2^\circ$  anisotropy in drop adhesion. The maximum degree of scale deflection is  $\approx 32^\circ$  when the drop rolls against the scales (Figure 2d), while no scale deflection is observed when the drop rolls toward the scales (Figure 2e). This directional scale deflection leads to a greater drop adhesion force when the drop rolls off against the scales, hence a greater roll-off angle in this direction.

From these experiments, we observe that the roll-off anisotropy of CNT scales is influenced by the geometry, compliance, and the morphology of the scales which influences the shape of the solid–liquid contact line and the ability of the scale to be deformed by the meniscus before depinning. We can capture these effects, and the scaling of the anisotropy, by a force balance model. At the macroscale (Figure 3a), the anisotropy is approximated by the difference in drop retention forces between the roll-off angles toward and against the scales,

$$\rho V g (\sin \alpha_2 - \sin \alpha_1) \approx F_{r,2} - F_{r,1} \quad (1)$$

where  $\alpha_1$  and  $\alpha_2$  are the roll-off angles toward and against scales, respectively;  $F_{1,r}$  and  $F_{2,r}$  are the corresponding drop retention force along the  $x$  axis (always parallel to substrate).

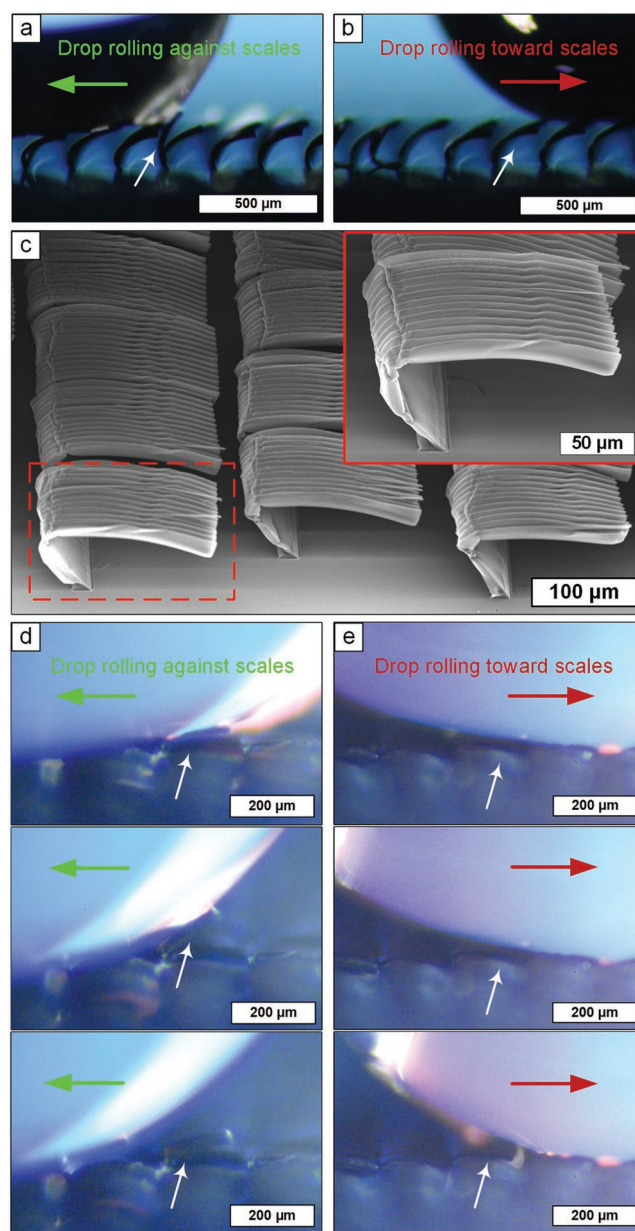


**Figure 2.** Compliance-mediated anisotropic adhesion on CNT scale surfaces. a,b) Optical images showing drop rolling on DVB-coated (unfolded) scales, exhibiting small deflection when rolling against scales (roll-off angle:  $6.7^\circ$ ) and no visible deflection when rolling toward scales (roll-off angle:  $3.4^\circ$ ). c) SEM images of folded DVB-coated CNT scale structures. d,e) Optical images showing drop rolling on folded scales, exhibiting large deflection when rolling against scales (roll-off angle:  $17.8^\circ$ ) and no visible deflection toward scales (roll-off angle:  $11.6^\circ$ ).

The drop retention difference must be approximately balanced by the adhesion force  $F_{r,d}$  between the drop and scale when the scale is deflected to its maximum angle (Figure 3b), which is represented by  $F_{r,d} \approx F_{r,2} - F_{r,1}$ . This adhesion force is estimated as the surface tension force at the contact line, projected in the drop rolling direction ( $x$  axis). The surface tension force at the drop–scale interface is

$$F_\sigma \approx \sigma L_c \sin \theta_{\text{rec}} \quad (2)$$

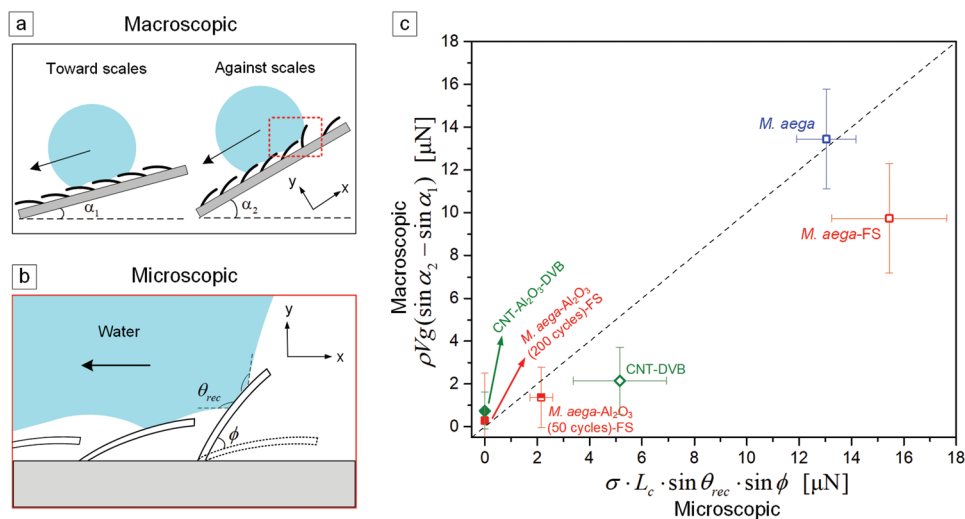


**Figure 3.** Validation with experimental data using model of compliance-mediated anisotropic roll-off. a) Schematic of macroscopic picture of drop roll-off toward and against scales. b) Schematic of microscopic picture of the drop-scale contact line on deflected scales. c) Macroscopic retention force as a function of the microscopic adhesion between the drop and the scale surfaces for pristine and coated *M. aega*, and synthetic CNT scales (FS: fluorosilane).

where  $\sigma$  is the surface tension of water ( $\sigma = 72 \text{ mN m}^{-1}$ ),  $L_c$  is the total contact line length on this scale surface (including the ridges), and  $\theta_{rec}$  is the measured local receding angle that the drop makes on the scale, which is dependent on the texture and surface energy of the surface. The direction of this resultant force  $F_\sigma$  is approximately normal to the scale surface (Figure S8, Supporting Information). Assuming the maximum scale deflection angle from its original horizontal position is  $\phi$ , the drop retention force coming from the scale deflection is

$$F_{r,d} \approx \sigma L_c \sin \theta_{rec} \sin \phi \quad (3)$$

If this approximate scaling is correct, we expect the relationship between macroscale and microscale forces to fall on a line of slope unity (Figure 3c),

$$\rho V g (\sin \alpha_2 - \sin \alpha_1) \approx \sigma L_c \sin \theta_{rec} \sin \phi \quad (4)$$

Experimental roll-off data measured from a pristine *M. aega* wing and the folded DVB-CNT synthetic scale surface is shown in Figure 3c, and falls near this trend line.

Clearly, the scale compliance influences adhesion anisotropy by affecting the maximum scale deflection angle  $\phi$  during drop rolling; to further demonstrate this using CNT scales, the compliance is tuned by conformably coating the CNTs with a thin layer of Al<sub>2</sub>O<sub>3</sub>.<sup>[30]</sup> The folded DVB-CNT scales have 4.0° roll-off anisotropy (Figure 4b; Movie S3, sample shown in Figure S9 in the Supporting Information). After coating the same sample with  $\approx 5 \text{ nm}$  (50 atomic layer deposition (ALD) cycles) of Al<sub>2</sub>O<sub>3</sub> (Figure S4, Supporting Information), followed by another DVB layer, it exhibits only 1° roll-off anisotropy (Figure 4c). The Al<sub>2</sub>O<sub>3</sub> coating increases the scale stiffness from 0.3 to 35 N m<sup>-1</sup> (Figure 4a). A drop rolling experiment performed on this sample shows nearly no scale deflection toward or against the scales (Movie S4, Supporting Information). This is because the Al<sub>2</sub>O<sub>3</sub> coating stiffens the scales such that the drop

pinning force is no longer large enough to deflect the scale. As a result, the scale surface behaves rigidly, and the drop experiences little difference in adhesion as it rolls toward and against scales. Similarly, *M. aega* scale samples treated with the same hydrophobic surface coating (fluorosilane) but having different engineered stiffnesses are also investigated and plotted in Figure 3c.<sup>[22]</sup> These data points generally follow the linear trend predicted by the model, supporting the implication that greater scale compliance results in greater drop adhesion anisotropy, and provides guidelines for increasing the anisotropy. This is also supported by the experimental observation that overlapping, unfolded CNT scales (Figure S2e,f, Supporting Information) exhibit smaller adhesion anisotropy (2°–3°) compared to those in Figure S7 (Supporting Information) due to constrained scale deflection.

Notably, pristine *M. aega* scale surfaces exhibit a much larger degree of roll-off anisotropy than the CNT-based synthetic counterparts. We believe this is because the petiole-like structure ( $\approx 10 \text{ }\mu\text{m}$  wide) at the base of each natural butterfly scale along with their small thickness ( $\approx 3 \text{ }\mu\text{m}$ ) allow for a large, reversible deflection angle ( $\approx 90^\circ$ ).<sup>[22]</sup> The dense packing of the overlapping scales and the flat scale geometry also contribute to the total liquid–solid contact length. Synthetic scales with small contact lengths (Figure S2a–c, Supporting Information) exhibited little or no anisotropy, which justified our segmented design of CNT scale geometries with flat upper portions. We expect that greater adhesion anisotropy of CNT scales could be achieved with a higher number of scales per area, and a smaller scale thickness.

In conclusion, we report a novel engineered 3D structured surface that possesses directional drop adhesion derived from the deflection of compliant scales. We outline the fabrication steps based on a strain-engineered CVD process of CNTs, followed by conformal polymer coatings. The resulting structures can be predictively designed and fabricated, along with tunable mechanical compliance and surface wettability. We demonstrate

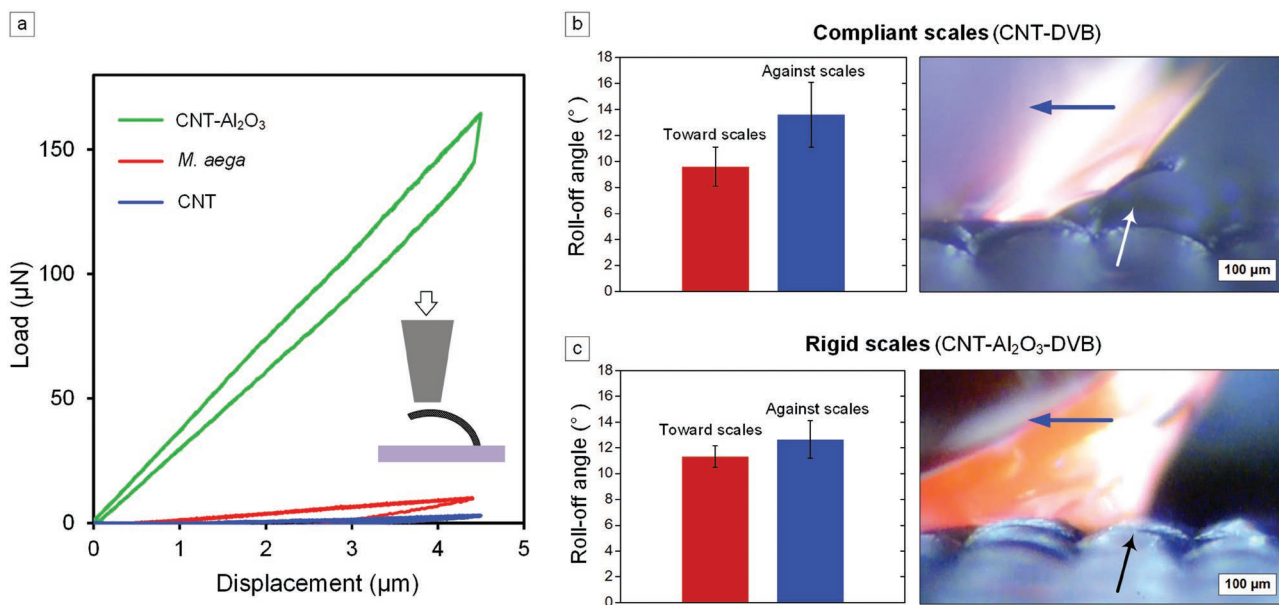


**Figure 4.** Influence of scale compliance on scale deflection during drop motion, and resultant adhesion anisotropy. a) Load-displacement curves of CNT scale arrays obtained using a 100  $\mu\text{m}$  radius flat tip, for as-grown CNT scales,  $\text{Al}_2\text{O}_3$ -coated CNT scales, and *M. aega* scales. Roll-off angles toward and against scales, and corresponding optical images at the instant of maximum deflection, comparing b) compliant and c) rigid synthetic scale surfaces.

that the compliance of scales plays a key role in enabling the scale deflection and therefore the drop roll-off anisotropy, which is a new concept in the synthesis of artificial anisotropic surfaces. Our synthetic scale surfaces with anisotropic adhesion are potentially useful for a wide range of applications, including artificial fluid transport devices, self-cleaning surfaces, and phase change energy conversion. Also, hierarchical patterning including interference lithography could add structural color to the scales for photonic applications.<sup>[25]</sup> In future work, the electrical conductivity of CNTs could enable additional control by electrowetting,<sup>[34]</sup> or via electrostatic actuation of the scales.<sup>[35]</sup>

## Experimental Section

**Substrate Patterning:** A (100) silicon wafer with 3000 Å of thermally grown oxide layer was used as the substrate for CNT scale growth. A 50 nm thick TiN layer was deposited on the substrate by sputtering (Endura 5500, Applied Materials). Subsequently, the TiN layer was patterned by photolithography, followed by a dry etching process using an etching system (Rainbow 9600, Lam Research) with  $\text{Cl}_2$  and  $\text{BCl}_3$  as the reaction gases for 30 s. After removing the photoresist by sonication in acetone for 15 min, a second photolithography step was performed to pattern the CNT catalyst by electron beam evaporation (VES-2550, Temescal) of the catalyst stack (10 nm of  $\text{Al}_2\text{O}_3$ , 1 nm of Fe) and a lift-off process.

**CNT Growth:** The catalyst/TiN wafer was cut into 15 mm  $\times$  15 mm pieces and placed in a furnace for CNT growth. The growth recipe started by flowing 100/400 sccm (standard cubic centimeters per minute) of  $\text{He}/\text{H}_2$  while heating the furnace to 758  $^\circ\text{C}$  over 10 min; then maintaining at 758  $^\circ\text{C}$  for 10 min with the same gas flow. Then the gas flow was changed to 100/400/100 sccm of  $\text{C}_2\text{H}_4/\text{He}/\text{H}_2$  for CNT growth. The growth step started at 758  $^\circ\text{C}$  for 3 min, then the temperature was increased to 765  $^\circ\text{C}$  for 40 s. Immediately after the growth step, the furnace lid was opened for rapid cooling. The furnace was cooled to <100  $^\circ\text{C}$  under the same gas flow, and then

the furnace was purged with 1000 sccm of He for 5 min before taking the sample out.

**Coating of DVB:** DVB was coated onto the CNT scale samples by iCVD conducted in a custom reactor. The peroxide initiator, TBPO (98%, Aldrich), was delivered into the reactor at a flow rate of 1 sccm. The monomer, DVB (80%, Aldrich), was vaporized in a glass jar by heating it to 60  $^\circ\text{C}$  at a flow rate of 0.5 sccm. An array of filaments suspended above the sample stage was resistively heated to 230  $^\circ\text{C}$  to cleave the labile bond of the initiator. The sample stage was back-cooled at 30  $^\circ\text{C}$  to promote the adsorption of the monomers to the surface. The pressure in the vacuum chamber was maintained at 800 mTorr.

**Coating of Fluorosilane:** The *M. aega* butterfly wings were exposed to a fluorosilane precursor (tridecafluoro-1,1,2,2 tetrahydrooctyl-trichlorosilane, Sigma-Aldrich) by placement next to 5  $\mu\text{L}$  of fluorosilane inside a vacuum desiccator for 4 h.

**ALD onto CNTs:**  $\text{Al}_2\text{O}_3$  was deposited by ALD (Gemstar, Arradance Corporation). Trimethylaluminum (TMA) and ozone ( $\text{O}_3$ ) were used as the metallorganic and oxidizing precursors, respectively. Using nitrogen as the carrier gas at a flow rate of 40 sccm, TMA and  $\text{O}_3$  were sequentially pulsed into the evacuated deposition chamber for 22 and 100 ms, respectively. The chamber was purged with a 90 sccm flow rate of nitrogen for 28 s following each precursor pulse. Deposition occurred at  $\approx 2\text{--}3$  torr and at a chamber temperature of 175  $^\circ\text{C}$ .

**Imaging of CNT Scales:** Imaging of CNT scales was performed using a scanning electron microscopy (SEM; Zeiss Merlin). No sample treatment was applied prior to SEM imaging.

**Nanoindentation:** The stiffness of each microscale was measured by nanoindentation (TI900, Hysitron). A flat sapphire indenter with 100  $\mu\text{m}$  diameter was indented on five scales at different locations to a maximum depth of 4500 nm at a 100  $\text{nm s}^{-1}$  indentation rate. The stiffness was determined by the average slope of the unloading curves.

**Measurement of Drop Roll-Off Angles:** CNT scale surface samples were placed on a flat plate (AP90, Thorlabs) connected to a motorized continuous rotation stage (CRI-Z7, Thorlabs). The plate was tilted from the horizontal plane at a rate of 1  $^\circ \text{s}^{-1}$  controlled using a motion control software APT (Thorlabs). A deionized water drop with a volume of  $3.2 \pm 0.4 \mu\text{L}$  was deposited onto the flat areas of scale surfaces using a high-resolution micropipette (0.5–10  $\mu\text{L}$  range, VWR). The stage tilt

angle where the water drop starts rolling off the sample was measured to be the roll-off angle. The roll-off angle was measured at five different locations on each sample.

**Optical Imaging of Drop Rolling on Scales:** A deionized water drop ( $\approx 3.2 \mu\text{L}$ ) was translated slowly on the flat areas of CNT scale surfaces by a thin wire, both toward and against the scales. Side-view optical imaging was taken using a digital SLR (Nikon D800) camera body connected to a Navitar 1-50486AD lens.

**Mechanical Crushing of CNT Scales:** The mechanical crushing of CNT scales was applied by placing 168 g weight on a glass slide, which was gently placed on top of the scales sample using a manual stage (PT1, Thorlabs) for contact. After contacting for 10 s, the weight was removed.

## Supporting Information

Supporting Information is available from the Wiley Online Library or from the author.

## Acknowledgements

H.Z. and S.J.P. contributed equally to this work. Financial support was provided by the Air Force Office of Scientific Research (FA9550-16-1-0011), the National Science Foundation (CMMI-1463344), and the MIT-Skoltech Next Generation Program (NGP). TiN/catalyst deposition and patterning were performed at the MIT Microsystems Technology Laboratories (MTL). Electron microscopy was performed at the MIT Center for Materials Science and Engineering (CMSE). Nanoindentation was performed at the MIT NanoMechanical Technology Laboratory (Nanolab). A portion of this work was performed at LLNL under the auspices of the US Department of Energy under contract DE-AC52-07NA27344.

Note: Equation (1) and Equation (4) were corrected after initial publication online.

## Conflict of Interest

The authors declare no conflict of interest.

## Keywords

adhesion, manufacturing, nanotube, surface, wetting

Received: November 28, 2018

Revised: January 25, 2019

Published online: February 13, 2019

- [1] S. Nishimoto, B. Bhushan, *RSC Adv.* **2013**, 3, 671.
- [2] M. K. Kwak, H.-E. Jeong, T.-I. Kim, H. Yoon, K. Y. Suh, *Soft Matter* **2010**, 6, 1849.
- [3] J. Lee, R. S. Fearing, K. Komvopoulos, *Appl. Phys. Lett.* **2008**, 93, 191910.
- [4] D. Xia, L. M. Johnson, G. P. López, *Adv. Mater.* **2012**, 24, 1287.
- [5] H. Chen, P. Zhang, L. Zhang, H. Liu, Y. Jiang, D. Zhang, Z. Han, L. Jiang, *Nature* **2016**, 532, 85.
- [6] D. Wu, J.-N. Wang, S.-Z. Wu, Q.-D. Chen, S. Zhao, H. Zhang, H.-B. Sun, L. Jiang, *Adv. Funct. Mater.* **2011**, 21, 2927.
- [7] Q. Wang, X. Yao, H. Liu, D. Quéré, L. Jiang, *Proc. Natl. Acad. Sci. USA* **2015**, 112, 9247.
- [8] Y. Zheng, X. Gao, L. Jiang, *Soft Matter* **2007**, 3, 178.
- [9] C. Liu, J. Ju, Y. Zheng, L. Jiang, *ACS Nano* **2014**, 8, 1321.
- [10] K. Watanabe, T. Hoshino, K. Kanda, Y. Haruyama, S. Matsui, *Jpn. J. Appl. Phys.* **2005**, 44, L48.
- [11] S. Tawfick, M. De Volder, D. Copic, S. J. Park, C. R. Oliver, E. S. Polsen, M. J. Roberts, A. J. Hart, *Adv. Mater.* **2012**, 24, 1628.
- [12] M. J. Hancock, K. Sekeroglu, M. C. Demirel, *Adv. Funct. Mater.* **2012**, 22, 2223.
- [13] L. Wen, Y. Tian, L. Jiang, *Angew. Chem., Int. Ed.* **2015**, 54, 3387.
- [14] S.-Z. Wu, D. Wu, J. Yao, Q.-D. Chen, J.-N. Wang, L.-G. Niu, H.-H. Fang, H.-B. Sun, *Langmuir* **2010**, 26, 12012.
- [15] N. A. Malvadkar, M. J. Hancock, K. Sekeroglu, W. J. Dressick, M. C. Demirel, *Nat. Mater.* **2010**, 9, 1023.
- [16] M. Prakash, J. W. M. Bush, *Int. J. Non-Linear Mech.* **2011**, 46, 607.
- [17] T. Kim, K. Y. Suh, *Soft Matter* **2009**, 5, 4131.
- [18] S. G. Lee, H. S. Lim, D. Y. Lee, D. Kwak, K. Cho, *Adv. Funct. Mater.* **2013**, 23, 547.
- [19] K.-H. Chu, R. Xiao, E. N. Wang, *Nat. Mater.* **2010**, 9, 413.
- [20] G. D. Bixler, B. Bhushan, *Soft Matter* **2012**, 8, 11271.
- [21] S.-H. Kang, T.-Y. Tai, T.-H. Fang, *Curr. Appl. Phys.* **2010**, 10, 625.
- [22] B. R. Solomon, A. T. Paxson, H. Zhao, S. Kim, D. Soto, Y. Zou, A. J. Hart, K. K. Varanasi, unpublished.
- [23] Z.-P. Yang, L. Ci, J. A. Bur, S.-Y. Lin, P. M. Ajayan, *Nano Lett.* **2008**, 8, 446.
- [24] K. Mizuno, J. Ishii, H. Kishida, Y. Hayamizu, S. Yasuda, D. N. Futaba, M. Yumura, K. Hata, *Proc. Natl. Acad. Sci. USA* **2009**, 106, 6044.
- [25] K. Cui, P. Lemaire, H. Zhao, T. Savas, G. Parsons, A. J. Hart, *Adv. Energy Mater.* **2018**, 8, 1801471.
- [26] M. De Volder, S. Park, S. Tawfick, A. J. Hart, *Nat. Commun.* **2014**, 5, 4512.
- [27] S. J. Park, H. Zhao, S. Kim, M. De Volder, A. John Hart, *Small* **2016**, 12, 4393.
- [28] N. Chakrapani, B. Wei, A. Carrillo, P. M. Ajayan, R. S. Kane, *Proc. Natl. Acad. Sci. USA* **2004**, 101, 4009.
- [29] B. Roman, J. Bico, *J. Phys.: Condens. Matter* **2010**, 22, 493101.
- [30] H. Zhao, C. Jacob, H. A. Stone, A. J. Hart, *Langmuir* **2016**, 32, 12686.
- [31] H. Sojoudi, S. Kim, H. Zhao, R. K. Annavarapu, D. Mariappan, A. J. Hart, G. H. McKinley, K. K. Gleason, *ACS Appl. Mater. Interfaces* **2017**, 9, 43287.
- [32] S. Kim, H. Sojoudi, H. Zhao, D. Mariappan, G. H. McKinley, K. K. Gleason, A. J. Hart, *Sci. Adv.* **2016**, 2, e1601660.
- [33] A. B. D. Cassie, S. Baxter, *Trans. Faraday Soc.* **1944**, 40, 546.
- [34] Z. Han, B. Tay, C. Tan, M. Shakerzadeh, K. Ostrikov, *ACS Nano* **2009**, 3, 3031.
- [35] F. A. Ghavanini, P. Enoksson, S. Bengtsson, P. Lundgren, *J. Appl. Phys.* **2011**, 110, 021101.